A physical-layer-aware multi-band optical network planning framework for rate-adaptive transceivers [Invited]

JASPER MÜLLER[1,2,*], GABRIELE DI ROSA[1], OGNJEN JOVANOVIC[1], MARIO WENNING[2,3], ACHIM AUTENRIETH[1], JÖRG-PETER ELBERS[1], AND CARMEN MAS-MACHUCA[2, 4]

[1] Adtran Networks SE, Martinsried/Munich, Germany
[2] Chair of Communication Networks, School of Computation, Information and Technology, Technical University of Munich (TUM), Germany
[3] Adva Network Security GmbH, Berlin, Germany
[4] Chair of Communication Networks, Universität der Bundeswehr München, Germany
[*] jasper.mueller@adtran.com

Flexible-grid elastic optical networks (EONs) have recently been widely deployed to support the growing demand for bandwidth-intensive applications. For cost-efficient scaling of the network capacity, multi-band systems are a promising solution. Optimized utilization of EONs is required to delay cost-extensive network upgrades and to lower cost and power consumption. Next-generation bandwidth-variable transceivers (BVTs) will offer increased adaptivity in symbol rate and modulation through techniques such as probabilistic shaping (PS). In this work, we investigate the impact of increased configuration granularity on optical networks. We account for practical implementation considerations of BVT configurations for estimating the required signal-to-noise ratio. Additionally, an optimization algorithm is presented that selects the most efficient configuration for each considered data rate and bandwidth combination. We utilize advanced quality of transmission estimation modeling to evaluate PS configurations in multi-band systems with optimized launch power distributions. We present results of network planning studies for C-band systems in a national and a continental optical backbone network topology considering different granularity of the configurations. Our analysis confirms that finer modulation-based rate-adaptivity results in substantial resource savings, decreasing the number of necessary lightpaths by at most 13% in C-band EONs. Additional savings are observed in multi-band systems, showing further increased savings in the number of required lightpaths of up to 20%. In contrast, increased symbol rate granularity only results in minor savings.

http://dx.doi.org/10.1364/jocn.514026

1. INTRODUCTION

Optical networks form the essential infrastructure for telecommunications, serving bandwidth-intensive applications such as high-resolution video streaming and 5G/6G. Addressing the increasing demands in data traffic requires cost-efficient solutions for upgrading network capacity. Flexible-grid Elastic Optical Networks (EONs) have gained widespread deployment in recent years, driven by advancements in bandwidth-variable transceivers (BVTs). A notable development in this context is the increase in symbol rates per wavelength, leading to coherent optical transceivers supporting rates of up to 140 GBd [1]. This enhancement contributes to reductions in both cost per bit and power consumption.

Optical long-haul backbone networks include demands between node-pairs whose distance can vary from less than one hundred to several hundred or even thousand kilometers. For efficient utilization of these networks, a variety of BVT configurations, defined as combinations of symbol rate and modulation format, are required. The increase in maximum data rate configuration of BVTs by increasing the symbol rate primarily improves efficiency for large traffic demands on short-distance links with high signal-to-noise ratio (SNR). Next-generation BVTs will enable fine granularity of configurations through advances in rate adaptivity for modulation and symbol rate [2]. For modulation-based rate-adaptivity, probabilistic shaping (PS) [3] established itself as a powerful solution. Although advances in rate adaptivity promise to enable cost-efficient capacity scaling using existing optical line system (OLS) resources, they come with additional

complexity for planning and operating networks.

In fixed-grid networks, potential benefits of increased rate adaptivity in modulation format using PS have been studied [4, 5]. Potential for significant resource savings has been shown with the use of advanced transmission modes using PS, limited to a channel spacing of 75 or 100 GHz [6]. Additionally, benefits of PS have also been evaluated for online planning in dynamic optical networks [7], and in multi-core fiber networks [8]. A software-defined networking-based optical network planning framework for the adaption of a PS-capable BVT according to optical SNR (OSNR) has been demonstrated in a field trial [9]. Several approaches to network planning for flexible-grid EONs have been proposed [10–13]. The benefits of high-symbol rate next-generation BVTs using traditional modulation formats have also been studied [14]. We presented network studies comparing different rate-adaptivity schemes using a practical approach to the estimation of the required SNR of PS transmission modes. The approach considers realistic implementation penalties and design choices using an optimization algorithm that selects BVT configurations for a targeted granularity in data rate and bandwidth [15]. Significant increases in capacity were achieved through increasing modulation-based rate-adaptivity, while higher symbol rate-adaptivity resulted in minor capacity gains.

Although the optimization of the utilization of existing OLS resources is the most cost-efficient way to increase capacity, the achievable gains are limited. In the long-term, upgrades of the OLS are necessary, either adding fiber-pairs or extending their range of operation beyond the C-band, the so called multi-band scenario [16]. Among the two options, the extension to multi-band systems is preferred for moderate capacity upgrades in the short- to medium-term, preventing costly deployment of additional fiber-pairs. Extensive research on multi-band transmission resulted in commercially available C+L-band systems. For the S-band on the other hand, the maturity of the technology is lower, which introduces challenges for short-term band activation. While erbium-doped fiber amplifiers (EDFAs) are used for the amplification of the C- and L-band, thulium-doped fiber amplifiers (TDFAs) are researched for S-band amplification [17]. Multi-band optical networks have been investigated from a network planning perspective, developing an integer-linear programming (ILP) formulation and heuristic algorithms considering ISRS [18, 19]. Multi-band deployment strategies have also been investigated [20]. Significant gains in network throughput have been shown in network planning studies for multi-band systems [12, 21]. Meaningful multi-band network planning studies require consideration of frequency-dependent physical parameters and inter-channel stimulated Raman scattering (ISRS) for accurate quality of transmission (QoT) estimation. Therefore, utilizing a closed-form ISRS Gaussian-Noise (GN) model is required [22]. Furthermore, the optimized frequency-dependent launch power values lead to significant gains in capacity compared to flat launch power spectra, as this enables pre-compensation of the ISRS effect and leads to a more flat SNR profile [23]. Non-uniform launch power is therefore preferred in multi-band transmission, but it comes at the cost of increased complexity for the QoT estimation. A semi-analytical approach involving solving the Raman differential equations and fitting frequency-dependent parameters was proposed to accurately capture the frequency dependent power profiles [24]. In our previous work, we have investigated the joined impact of emerging technologies such as PS, multi-band and multi-wavelength sources showing significant capacity gains and reductions in the required number of lightpaths (LPs) [25].

In this work, we extend our previous investigation of the impact of an increased configuration granularity on optical networks [15]. The work has been extended to include rate-adaptivity studies for multi-band scenarios. As 12.5 GHz spacing has been identified as a good trade-off for symbol rate granularity. This has been selected as an additional baseline scenario to ensure a fair comparison. Particular consideration has been put into QoT estimation. Frequency-dependent parameters assuming the ITU-T G.652.D specification [26] have been considered. The closed-form GN model considering ISRS and modulation format dependency is utilized together with frequency dependent parameters, fitted to numerically computed power profiles [22].

We take a practical forward error correction (FEC) code [27] into account as well as realistic implementation penalties and design choices. PS transmission modes with base constellations of up to 64 QAM, as implemented in commercially available BVTs, are considered. For further preparation of the network study, an optimization algorithm that selects BVT configurations for a targeted granularity in data rate and bandwidth is presented. For each data rate and bandwidth combination, the algorithm chooses the configuration leading to the lowest required SNR.

A physical-layer-aware network planning algorithm [25] for flexible-grid EONs is used to conduct a network planning study on the Nobel-Germany (Germany) and the Nobel-EU (EU) topologies [28]. The results are compared for different symbol rate-adaptivity schemes in C-band systems and for the symbol rate-adaptivity of 12.5 GHz in multi-band systems, i.e., C+L-band and C+L+S-band. We show that an increased modulation-based rate-adaptivity leads to significant savings in required number of LPs of up to 13% in C-band systems and up to 20% in multi-band systems. Furthermore, underprovisioning is reduced by up to 10 percentage points for high requested traffic, thereby leading to more efficient utilization of the available spectrum. An additional increase in symbol rate granularity from 37.5 GHz to 12.5 GHz offers moderate improvements of up to 4% less underprovisioning. On the other hand, a further increased symbol rate granularity achieves little benefits while significantly increasing the planning complexity.

The main contributions of this work can be summarized as follows:

- A practical approach to computing the required SNR of PS-QAM configurations (Section 2.A), a pre-selection algorithm (Section 2.B) for consideration in network planning studies and a framework for accurate QoT estimation in multi-band scenarios (Section 2.C) are presented,,

- C-band, C+L-band and C+L+S-band network planning studies comparing different symbol and modulation-based rate-adaptivity scenarios are presented in Section 3.

2. PHYSICAL-LAYER CONSIDERATIONS

In physical-layer-aware network planning, feasible configurations of an LP with a given data rate are determined by their minimum SNR necessary for error-free transmission (required SNR). The required SNR is determined by the theoretical SNR limit, influenced by the forward-error-correction overhead (FEC_{OH}) as well as transceiver (TRx) implementation penalties which are dependent on the modulation format and the symbol rate. In Section 2.A we present the calculation of an upper bound of the required SNR for all configurations across different symbol rates

and probabilistically shaped modulation formats with variable base constellation size. In Section 2.B, the results are used to select only the relevant configurations for a targeted granularity in data rate and symbol rate steps.

The expected SNR of a LP is computed from TRx impairments, linear impairment, i.e., amplified spontaneous emissions (ASE) and non-linear interference (NLI), as

$$\text{SNR}^{-1} = \text{SNR}_{TRx}^{-1} + \text{SNR}_{ASE}^{-1} + \text{SNR}_{NLI}^{-1}. \qquad (1)$$

Particular care is required for computing impairments related to NLI. Closed-form GN models are the state-of-the art for computation of the NLI in network planning studies. These analytical models have been derived through approximations and assumptions. In Section 2.C we present the NLI computation engine used for the network planning studies.

A. Required SNR of Probabilistically Shaped Modulation Formats

Probabilistically shaped quadrature amplitude modulation (PS-QAM) allows tuning the number of information bits per QAM symbol, i.e., the entropy of the transmitted signal denoted by H. This enables fine adaptation of the transmitted net data rate (DR_{net}) without requiring the implementation of multiple FEC codes with variable overhead. PS-QAM requires a distribution matcher and dematcher, which increases the complexity of the transceiver. Also, as the transmit data rates increase above Tbit/s, efficient hardware implementation could be difficult to realize [29, 30]. However, it should be mentioned that PS can be found in high-end commercial DSP implementations [1]. It was shown that in practice combining PS-QAM with a single high-performance soft-decision FEC (SD-FEC) code offers better performance and finer granularity compared to uniform QAM combined with variable-rate FEC codes [3]. For successful network planning, the achieved DR_{net} and the related signal quality required at the receiver for each configuration when using PS-QAM should be accurately evaluated. For each configuration, DR_{net} is computed for dual-polarization signals as [3]:

$$DR_{net} = 2R_{sym} \left[H - \log_2(M) \left(1 - \frac{1}{1 + FEC_{OH}} \right) \right], \qquad (2)$$

where M is the size of the base QAM constellation, H is the entropy of the signal and R_{sym} is the symbol rate.

When observing Eq. 2, two essential conclusions have to be made: 1) For a fixed non-ideal FEC code, the information rate suffers a loss proportional to $\approx \log_2(M)$ for larger base constellations [31]; and 2) The DR_{net} increases with the increase of the constellation entropy H, with the upper bound being uniform M-QAM, $H = \log_2(M)$, leading to:

$$DR_{net} = \frac{2R_{sym} \log_2(M)}{1 + FEC_{OH}}. \qquad (3)$$

If error-free operation is preserved, point 2) shows effective increase in the exchanged amount of information. Even though higher order base modulation formats increase the maximum DR_{net}, they have greater implementation penalties. This fact, combined with point 1), drives the use of the smallest base constellation that can provide the required entropy as the optimal implementation choice in most practical cases. Clearly, for the same symbol rate, configurations with higher entropy require better received signal quality.

Normalized generalized mutual information (NGMI) [32] and the asymmetric information [33] are information theoretical

Algorithm 1. Pre-selection Algorithm

Input: Configurations $\mathcal{C}$, considered data rates $\mathcal{D}$ and symbol rates $\mathcal{S}$
Output: Pre-selected configurations $\mathcal{C}_{considered}$
1: **function** PRE-SELECT($\mathcal{C}, \mathcal{D}, \mathcal{S}$)
2:     $\mathcal{C}_{considered} \leftarrow \varnothing$
3:     **for** $d \in \mathcal{D}$ **do**
4:         **for** $s \in \mathcal{S}$ **do**
5:             $c_{opt} \leftarrow c \in \mathcal{C}_{s,d}$ with lowest SNR_{req}
6:             add c_{opt} to $\mathcal{C}_{considered}$
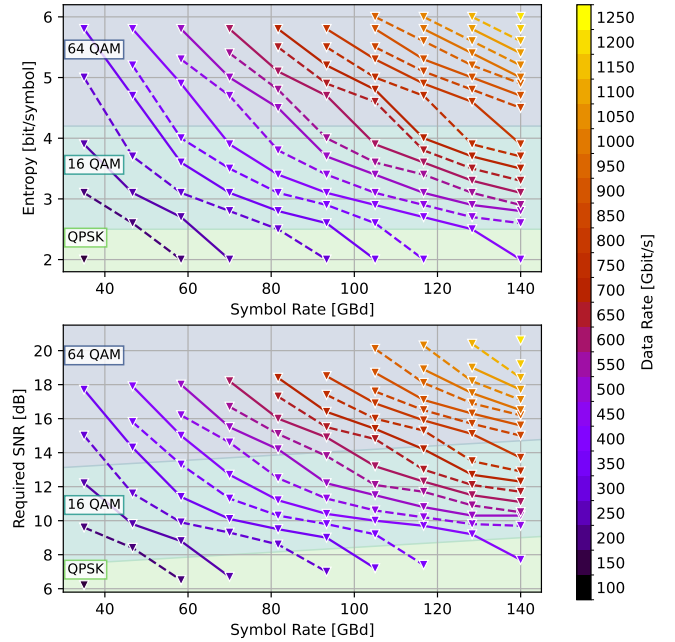7:   **return** $\mathcal{C}_{considered}$

Fig. 1. Entropy H (top) and required SNR (bottom) over symbol rate R_{sym} for configurations with 50 Gbit/s data rate granularity and 12.5 GHz bandwidth slot granularity. The single point in the lower left side of the plots represents the 100 Gbit/s QPSK configuration. Moving towards the upper left of the plot, each line represents a 50 Gbit/s step. A triangle marks the considered configurations for each data rate. The shaded areas indicate the different base constellations.

metrics designed to precisely predict if decoding a received signal will be error-free after applying a given SD-FEC code. Theoretically, these quantities are excellent system performance indicators regardless of the considered modulation format and FEC_{OH}. However, practically, it is challenging to translate them into network-level requirements. In that case, pre-FEC bit-error-ratio (BER) and required SNR are more readily-available and intuitive performance metrics. For traditional systems with hard decoding FEC (HD-FEC), the pre-FEC BER proved to be an accurate performance indicator. However, the use of PS-QAM and SD-FEC leads to variable pre-FEC BER thresholds for different modulation formats. This variation increases for higher FEC_{OH} [32]. However, for $FEC_{OH} \leq 50\%$, the pre-FEC BER still provides fairly consistent predictions for different PS-QAM configurations [33].

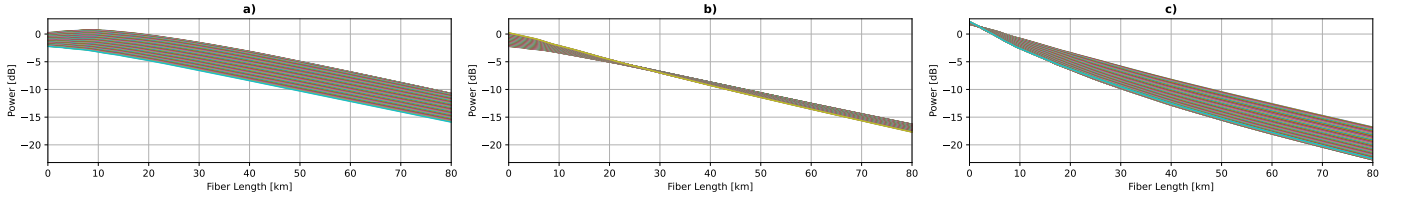We consider an established FEC code [27] with $FEC_{OH} = 27\%$

Fig. 2. Fitted power profile of C+L+S-band transmission for **a)** L-band channels, **b)** C-band channels and **c)** S-band channels, respectively.
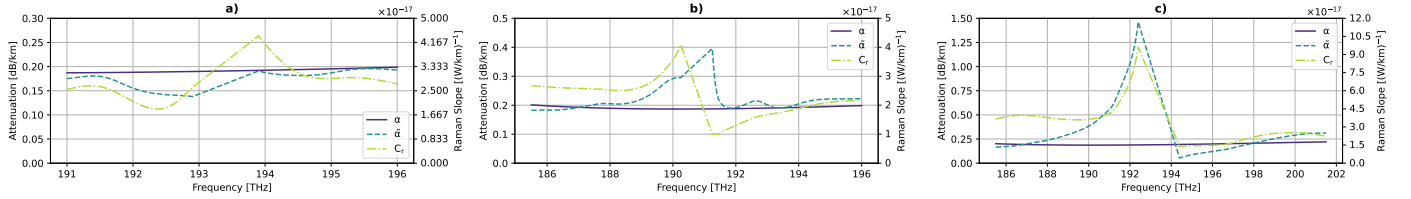

Fig. 3. Frequency dependent parameters α, $\tilde{\alpha}$ and C_r for **a)** C-band transmission, **b)** C+L-band transmission, **c)** C+L+S-band transmission.

and pre-FEC BER threshold = 3.5%. This threshold proved to be a worst case pre-FEC BER value that guarantees successful decoding over the considered modulation formats. Assuming for all cases this worst case value translates into adding small modulation-specific SNR margins which are expected to vary slightly across configurations. Once the PS-QAM configuration is determined, the pre-FEC BER threshold is converted into the required SNR assuming additive white Gaussian noise. This enables the use of SNR for quality of transmission estimation, which significantly simplifies the network planning. Implementation penalties for the base modulation format are included in the required SNR calculation. These penalties are 1 dB for QPSK, 1.5 dB for 16 QAM and 2 dB for 64 QAM. A symbol rate dependent implementation penalty is also included by assuming 0.5 dB penalty per 35 GBd and starting with no penalty for a 35 GBd LP, this penalty is computed as

$$\text{Penalty}_{R_{\text{sym}}} = 0.5 \, \text{dB} \frac{R_{\text{sym}} - 35 \, \text{GBd}}{35 \, \text{GBd}}. \qquad (4)$$

B. Pre-selection of Configurations

We consider next-generation BVTs to allow for fine-granularity modulation-based rate-adaptivity (0.1 bit/symbol steps between 2 and 6 bit/symbol of entropy) and a tunable symbol rate between 35 and 140 GBd in steps of 2 GBd [2]. Thereby, a total of 2080 different configurations exist. The number of useful distinct configurations depends on the targeted data rate granularity of the network operator as well as the spectral slot width in the network. The most common configurations utilize a symbol rate of 35 GBd or multiples of it, as it corresponds to 100/200/300 Gbit/s for QPSK/16 QAM/64 QAM. Flexible-grid optical networks are usually operated with a spectral slot width of 12.5 GHz, while we assume a slot width of 3.125 GHz will be possible in next-generation EONs. Therefore, we investigate three different symbol rate granularities, while considering a data rate granularity of 50 Gbit/s in the network planning studies.

A pulse roll-off of 5% determines the relationship between symbol rate and channel bandwidth. The slot of a channel is chosen as the lowest number of spectral slots the channel bandwidth fits into. E.g., a 35 GBd channel has a bandwidth of

36.75 GHz and occupies three spectral slots of 12.5 GHz, i.e., a slot of 37.5 GHz. For the definition of the symbol rate-adaptivity scenarios, we consider different numbers of bandwidth slot options uniformly distributed between the minimum of 37.5 GHz and 150 GHz and their corresponding symbol rates uniformly distributed between 35 GBd and 140 GBd. The following symbol rate-adaptivity scenarios are investigated:

- Scenario **1)** 4 possible bandwidth slot options of 37.5, 75, 112.5 and 150 GHz,

- Scenario **2)** 10 possible bandwidth slot options with 12.5 GHz resolution,

- Scenario **3)** 37 possible bandwidth slot options with 3.125 GHz resolution.

Scenarios considering the three modulation formats QPSK, 16 QAM and 64 QAM, denoted as *Uniform*, and utilizing PS QAM modulation, denoted as *PS*, are compared. The required SNR (SNR_{req}) is computed as described in Section A. In order to find the most useful configurations in the *PS* scenario, for each symbol rate-adaptivity scenario, we start with all combinations of the considered symbol rates and possible entropies. For each of these configurations, we consider the effective data rate (DR_{eff}), defined as DR_{net} rounded down to the next 50 Gbit/s step.

The set of considered configurations $\mathcal{C}_{considered}$ are chosen by the pre-selection algorithm Alg. 1. For a given scenario, we define $\mathcal{D}$ and $\mathcal{S}$ as the set of considered data rates and symbol rates, respectively. $\mathcal{C}_{s,d}$ is the set of configurations with DR_{eff} = d and $R_{\text{sym}} = s$. Note that not all combinations of d and s are achievable with the considered modulations, e.g. for $d >$ 300 Gbit/s and $s = 35$ GBd $\mathcal{C}_{s,d}$ will be empty. The considered configurations are selected such that for each d, s combination, the configuration that leads to the lowest SNR_{req} out of $\mathcal{C}_{s,d}$ is added to $\mathcal{C}_{considered}$.

For Scenario **1)**, **2)** and **3)**, Alg. 1 selects a number of 44, 115 and 423 considered configurations, respectively. Fig. 1 shows entropy and required SNR over symbol rate for all data rate steps for Scenario **2)**. The required SNR of an LP can be finely tuned with the available combinations of entropy and symbol rate to closely match the LP's SNR.

C. Quality of Transmission (QoT) Estimation

The closed-form GN models for NLI computation have experienced a plethora of iterations in the past few years, aiming at generalizing their validity and improving their estimation accuracy. We utilize a model that takes into account ISRS as this is a major non-linear effect in multi-band systems [24].

An important element of the GN model for our evaluation is the modulation format correction factor [34]. It is important to be considered for a fair evaluation of PS-QAM configurations, as base constellations lead to lower NLI than their shaped counterparts.

Finally, frequency-dependent physical parameters of the optical fiber are an important factor to consider for accurate ASE and NLI computation in multi-band systems. The spatially resolved power profile of the channels propagating over the fiber is heavily affected by ISRS. While the power profile can be accurately modeled by an analytical formula when assuming a flat launch power spectrum [24], a semi-analytical approach consisting of computing the power profile by numerically solving the Raman differential equations and fitting the frequency-dependent parameters is required for non-uniform launch power distributions. The parameters α, $\tilde{\alpha}$ representing the attenuation, and the Raman slope parameter C_r are fit in the formula given by [24] (Eq.17).

Considering launch power offsets and tilts per band increases the flatness of the achieved QoT over all frequencies and leads to increased capacity [23]. We consider the launch power values as presented in [23]. The power profiles have been computed numerically considering a 50 GHz grid on an 80 km span of ITU-T G.652.D fiber (Fig. 2). Utilizing least squares fitting, the parameters as shown in Fig. 3 have been obtained. As the fitting of α had minimal impact on the fit, we opted to fix the parameter to the actually observed attenuation. The closed-form GN model requires a reference frequency in the center of the spectrum. At this frequency, the parameters $\tilde{\alpha}$ and C_r have no effect. We further observed minimal effect of these parameters within 500 GHz (1 THz for C+L+S band) to either side of the reference frequency. Therefore, fitting the parameters in this area is difficult while having minimal effect on the power profile fit. We interpolate the parameters linearly within this range of frequency. Due to ISRS, the operation of partially loaded multi-band systems is difficult as the addition of LPs will change the power profiles of all channels. Therefore, we assume ASE-loading of the spectrum for unused frequencies.

3. NETWORK PLANNING STUDY

In this section, the impact of modulation and symbol rate adaptivity is analyzed in a network planning study on two publicly available network topologies of different characteristics (Tab. 1), describing a national (Germany) and a continental (EU) backbone network [28].

Topology	# Nodes	# Links	# Demands	Avg. Node Degree	Avg. Path Length
Germany [28]	17	26	136	3.05	420 km
EU [28]	28	41	378	2.92	1100 km

Table 1. Core network topologies considered.

A. Setup

For the planning scenarios, the links are assumed to be standard single-mode fiber (SSMF) links [26], consisting of 80 km spans with perfect compensation of the fiber attenuation at the end of each span by an EDFA for C and L-band and a TDFA for S-band. We assume 5 dB, 5.5 dB and 7 dB noise figures for the amplifiers in C-,L-, and S-band, respectively [12]. The transmit power spectral density is set according to [23]. As baseline scenarios, we consider configurations with QPSK, 16 QAM and 64 QAM as modulation formats and symbol rate granularity as from Scenario **1)** and **2)** called *Uniform 37.5 GHz* and *Uniform 12.5 GHz*. These baselines are compared to scenarios using PS QAM modulation as detailed in Section 2.B with symbol rate granularities according to Scenario **1)**, **2)** and **3)**, named *PS 37.5 GHz*, *PS 12.5 GHz* and *PS 3.125 GHz*, respectively. We assume 5 THz of usable bandwidth in each band with 500 GHz of guard band in between. Therefore, we consider flexible grid networks, with 400 frequency slots per band of 12.5 GHz each. For Scenario **3)** 1600 frequency slots of 3.125 GHz are considered per band.

Aggregated traffic requests for source-destination node pairs are considered as demands. The demands are weighted according to a traffic model based on the number of data centers and internet exchange points in each ROADM location [12]. To vary the network traffic demands, the individual demands are scaled by the same factor in order to reach different levels of aggregate requested network traffic (ART). The routing, configuration, and spectrum assignment (RCSA) algorithm [12] considers $k = 3$ shortest-path routing. The spectrum is assigned according to the first-fit algorithm. The configurations of each LP are chosen in order to minimize the number of required LPs as primary and the used bandwidth as secondary objective. Candidate configurations are chosen based on the end-of-life (EoL) SNR, assuming the worst-case of a full spectrum of gaussian modulated interfering channels in order to model the ASE loading. The EoL SNR is computed for each configuration that is valid with respect to the linear SNR and can be placed on the spectrum. Configurations with a required SNR threshold lower than the computed SNR are considered [25]. For the analysis of the results of the network planning study, we compare provisioned traffic, number of deployed LPs and underprovisioning ratio (UP) [12] for the different scenarios.

B. C-band Results

We first start with the evaluation of different rate-adaptivity scenarios in C-band networks. The network planning results for the Germany topology are shown in Fig. 4. We observe that the *Uniform 37.5 GHz* scenario shows slightly higher overprovisioning up to 150 Tbit/s of ART than other scenarios (Fig. 4 **a)**). Overprovisioning occurs because the demanded data rates are on a continuous scale, therefore the next higher feasible data rate will be chosen to fulfill the demand. Since the *Uniform 37.5 GHz* scenario only considers three modulation formats and four symbol rate options some data rates cannot be achieved. Therefore, slightly increased overprovisioning is observed. For high ART, it can be seen that the provisioned traffic of the baseline scenario drops below the ART first. The provisioned traffic of all three rate adaptivity scenarios is comparable over all ART values with *PS 12.5 GHz* and *PS 3.125 GHz* provisioning slightly more traffic than *PS 37.5 GHz* for ART above 200 Tbit/s.

The *Uniform* scenario requires a larger number of LPs to fulfill all demands. At 150 Tbit/s, *Uniform 37.5 GHz* requires up to 13% more LPs than the *PS* scenarios (Fig. 4 **b)**). For the *PS* scenarios,
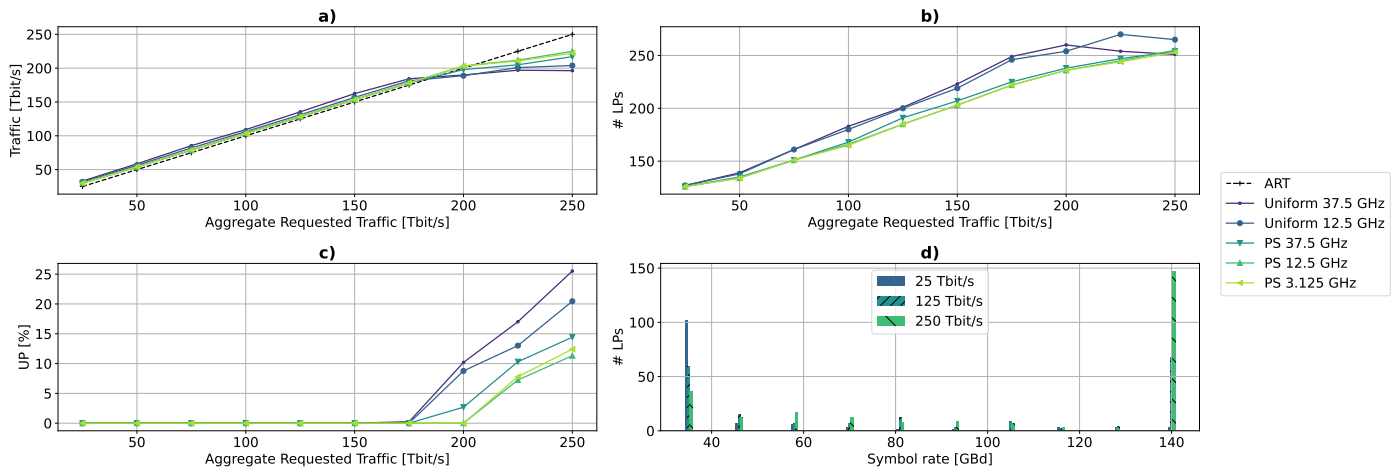
Fig. 4. Planning results on Germany: **a)** provisioned traffic, **b)** number of deployed LPs, **c)** underprovisioning, and **d)** symbol rate distribution for *PS 12.5 GHz*.
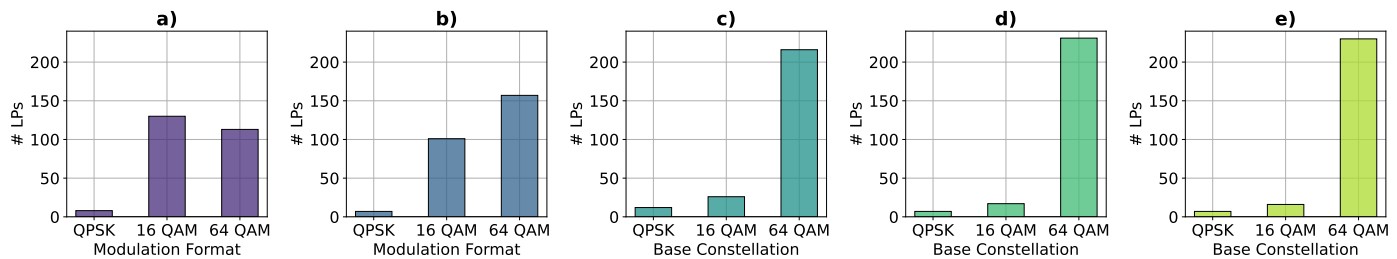

Fig. 5. Number of LPs per base constellation on Germany for **a)** *Uniform 37.5 GHz*, **b)** *Uniform 12.5 GHz*, **c)** *PS 37.5 GHz*, **d)** *PS 12.5 GHz* and **e)** *PS 3.125 GHz* at 250 Tbit/s ART.

it can be seen that for ART below 200 Tbit/s *PS 37.5 GHz* requires up to 5% more LPs than *PS 12.5 GHz* and *PS 3.125 GHz* while at the highest considered ART values a slightly lower number of LPs is deployed. Fig. 4 **c)** explains this as it can be seen that the UP for *PS 37.5 GHz* is up to 4% higher than the UP that is observed for *PS 12.5 GHz* and *PS 3.125 GHz*. The baseline scenarios show significantly higher UP of up to 14 percentage points above the *PS* scenarios for ART above 150 Tbit/s.

These results show a significant benefit when considering *PS* over the baseline scenario as the number of required LPs and UP is noticeably reduced while a higher ART can be provisioned without underprovisioning. The benefit of using a higher symbol rate granularity is relatively minor as at 250 Tbit/s ART the difference in UP between Scenario *PS 37.5 GHz* and *PS 3.125 GHz* is 4 percentage points. The comparison of *PS 12.5 GHz* and *PS 3.125 GHz* shows that *PS 3.125 GHz* requires up to 2% less LPs to provision all demands for ART up to 200 Tbit/s. For higher ART values, the heuristic planning algorithm leads to a slightly better performance of the *PS 12.5 GHz* scenario, due to the specific order demands are fulfilled in. Reordering the demands by requested data rate in descending order would lead to the expected outcome of *PS 3.125 GHz* slightly outperforming *PS 12.5 GHz* at the expense of a higher number of underprovisioned demands. We leave the optimization of demand ordering for future research.

Fig. 4 **d)** shows the distribution of symbol rates over all LPs for *PS 12.5 GHz* over different levels of ART. It can be seen that for a low level of ART (25 Tbit/s) the minimum considered symbol rate of 35 GBd is chosen while for higher ART, most LP configurations are either at 35 GBd or close to the maximum

considered symbol rate of 140 GBd. As the high symbol rate configurations are generally more spectrally efficient due to the absence of guard-bands between multiple channels, these are chosen until one last LP is sufficient to fulfill the remaining requested traffic for a demand. This last LP will be chosen with the minimal possible symbol rate in order to minimize spectral usage. These results explain the lower differences between the rate adaptivity scenarios with different symbol rate granularities when compared to the benefits gained by modulation-based rate-adaptivity, as the minimum and maximum considered symbol rates will be chosen for the majority of the deployed LPs.

In Fig. 5 the distribution of the modulation format/base constellation of placed LPs is shown at 250 Tbit/s ART on the Germany topology for each scenario. We observe that for the *Uniform 12.5 GHz* scenario, significantly more 64 QAM channels are placed than for *Uniform 37.5 GHz*. In contrast, more than 75 % of LPs use a 64 QAM base constellation in the *PS* scenarios, implying an entropy larger than 4 bit/symbol. Therefore, the configuration options between 4 and 6 bit/symbol are particularly impactful in the observed increased capacity of *PS* over *Uniform* on the Germany topology. Minor differences are observed between the symbol rate granularities of *37.5 GHz* and *12.5 GHz*, while *3.125 GHz* does not improve the distribution further. In general, the *PS* scenarios improve spectral efficiency significantly compared to the *Uniform* scenario.

In comparison, as a continental network, the EU topology has a larger number of nodes and demands than the Germany network and more than double the average path length (Tab. 1). The longer paths lead to a lower capacity in this network, considering the used traffic model. The network planning results
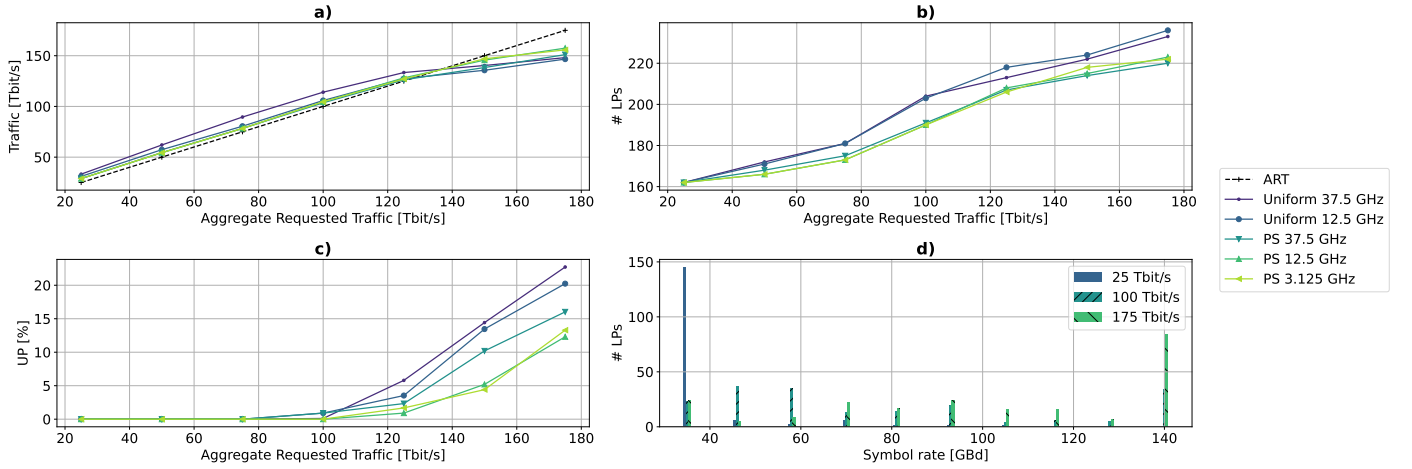
Fig. 6. Planning results on EU: **a)** provisioned traffic, **b)** number of deployed LPs, **c)** underprovisioning, and **d)** symbol rate distribution for *PS 12.5 GHz*.
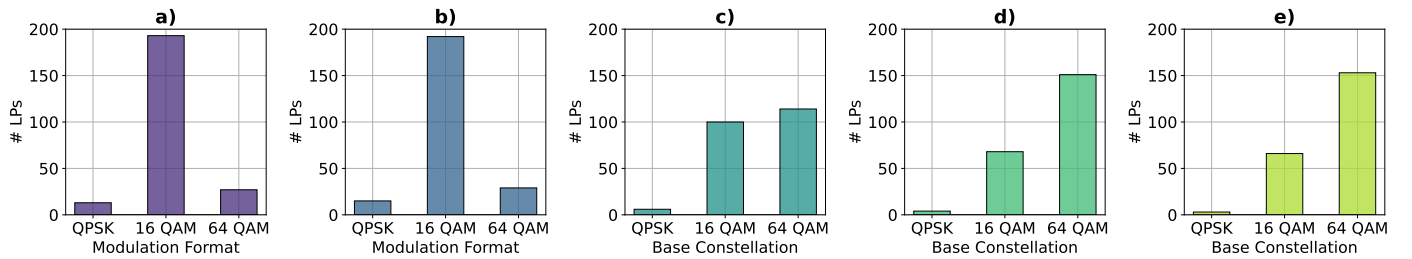

Fig. 7. Number of LPs per base constellation on EU for **a)** *Uniform 37.5 GHz*, **b)** *Uniform 12.5 GHz*, **c)** *PS 37.5 GHz*, **d)** *PS 12.5 GHz* and **e)** *PS 3.125 GHz* at 175 Tbit/s ART.

for the EU network as shown in Fig. 6 are consistent with our observation on the Germany topology. A large difference between the *Uniform* and the *PS* scenarios is observed as we see more overprovisioning for low ART, until the provisioned traffic drops below ART as the requested traffic cannot be fulfilled at ART values above 75 Tbit/s (Fig. 6 **a)**). The *Uniform* scenarios require up to 8% more LPs than the *PS* scenarios (Fig. 6 **b)**) and the UP is up to 10 percentage points higher (Fig. 6 **c)**). The differences between the different *PS* scenarios are again smaller. Fig. 6 **d)** shows that 35 GBd configurations are used almost exclusively for low ART of 25 Tbit/s in *PS 12.5 GHz*. For higher ART values the concentration of configurations at the lower and upper end of the considered symbol rates is less pronounced than it is for Germany. The significantly higher number of demands in the EU network lead to a lower requested traffic per node pair on average. Therefore the symbol rate options, that are not at the extremes, are chosen comparably more often for the EU network than for Germany.

The modulation distributions on the EU topology at 175 Tbit/s (Fig. 7) show that compared to Germany, 16 QAM is used more often while a lower amount of 64 QAM LPs are placed. We observe that only a few 64 QAM channels are placed in the *Uniform* scenarios with less difference between the symbol rate granularities *37.5 GHz* and *12.5 GHz*. This is a result of the longer average path length and different path length distribution lowering the impact of symbol rate granularity in the *Uniform* scenarios. In contrast, up to around two thirds of the LPs use a 64 QAM base constellation for the *PS* scenarios. Consistent with the results on the Germany topology, a difference is observed between *37.5 GHz* and *12.5 GHz* symbol rate granularity,

while *3.125 GHz* does not offer additional benefits. Therefore, we conclude that the symbol rate granularity of 12.5 GHz is sufficient and represents a good trade-off between complexity of the planning algorithm and optimized spectrum utilization.

C. Multi-Band Results

For the Multi-band evaluation, we fix the symbol rate granularity to 12.5 GHz, as previously confirmed to be a good trade-off. We compare *PS* and *Uniform* in C-band, C+L-band and C+L+S band transmission scenarios at different ART levels on the EU topology in Fig. 8. With the addition of bands, significantly higher levels of ART can be provisioned in the network (Fig. 8 **a)**). The results confirm the advantage of *PS* over *Uniform* shown in the previous section, also in multi-band scenarios as the *PS* scenarios consistently exhibit lower UP than the *Uniform* scenarios with a maximum of 8% difference observed for C+L-band. In the *PS* scenarios 25 Tbit/s more ART can be provisioned without exhibiting underprovisioning (Fig. 8 **b)**). With higher ART values, the savings in the number of required LPs for *PS* over *Uniform* increases until the ART cannot be fully provisioned to up to 15% for C+L+S-band transmission at 350 Tbit/s. While the addition of bands provides higher capacity gains than just the change to optimized *PS* configurations, both of these emerging technologies synergize well, as the benefits of *PS* increase with additional bands. Therefore, utilizing *PS* configurations can support achieving a decreased cost and power consumption per bit by saving significant amounts of LPs and therefore transponders in the network.

Due to the higher level of ART that can also potentially be provisioned without UP, *PS* can be utilized to postpone upgrad-
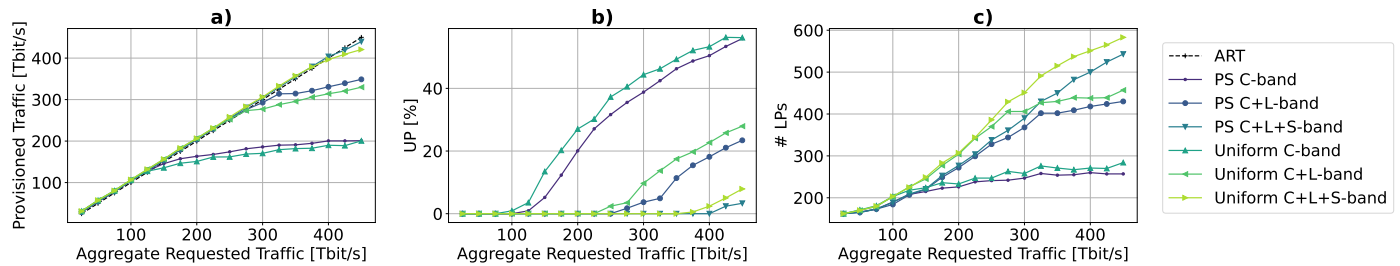
Fig. 8. Planning results on Nobel-EU topology. **a)** Provisioned traffic, **b)** underprovisioning (UP) and **c)** number of provisioned LPs over aggregate requested traffic (ART).
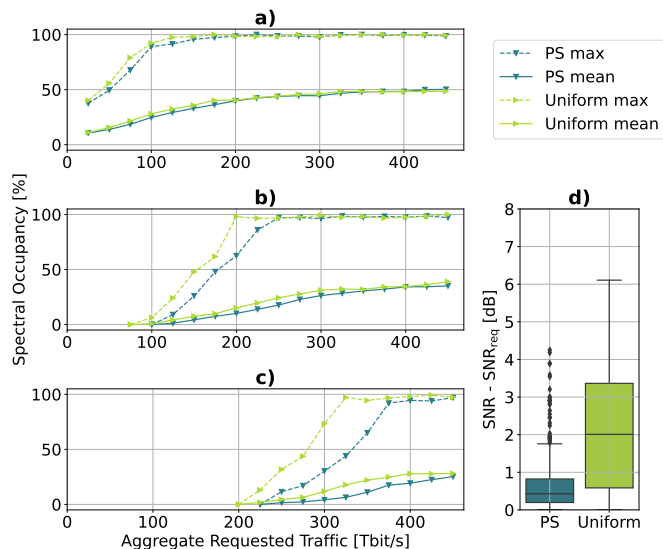

Fig. 9. Mean and maximum link spectrum used over aggregated requested traffic in **a)** C-band, **b)** L-band and **c)** S-band and (d) SNR margin ($SNR_{req} - SNR$) distribution for the C+L+S-band scenario at 450 Tbit/s ART.

ing the OLS for additional bands. Fig. 9 shows the average and maximum link-band utilization in the C+L+S band scenarios. The large difference between maximum and average utilization is due to the shortest path routing. While different routing and spectrum assignment approaches can be utilized for a more balanced link-spectrum utilization, this comes at the expense of higher average path length and therefore less spectrally efficient configurations, a higher number of links used per LP and higher latency. Therefore, as the benefit in operations is questionable, we decided to utilize shortest path routing. comparing the band utilization for *Uniform* and *PS*, we see that *PS* delays the usage of the L-band (Fig. 9 **b)**) and the S-band (Fig. 9 **c)**). (Fig. 9 **d)**) shows the distribution of the difference between the SNR of an LP and the SNR_{req} of its configuration. The difference is significantly lower for *PS* with a median of around 0.5 dB as compared to *Uniform* with a median of 2 dB. *PS* enables more efficient usage of the available QoT by choosing configurations with an SNR_{req} closer to the actual SNR. The results for multi-band systems on the Germany topology are not shown as they are consistent with the results presented for EU, improving the savings in the number of required LPs to up to 20% for C+L+S-band.

4. CONCLUSIONS

We presented a physical-layer-aware optical network planning framework to evaluate the benefits of rate-adaptive transceivers in C-band and multi-band optical transport networks. We calculated the SNR requirements of bandwidth-variable transceiver configurations based on probabilistically shaped modulation formats by taking into account practical implementation aspects for the FEC as well as realistic transceiver implementation penalties. An optimization algorithm that selects the most efficient BVT configurations for a targeted granularity in data rate and bandwidth is presented. The QoT estimation for the planning studies considers ISRS, modulation format dependency and an optimized non-uniform launch power distribution to ensure a fair and meaningful comparison of considered rate-adaptivity schemes.

Results from a physical-layer-aware network planning study on national and continental optical backbone network topologies considering C-band transmission show that increased modulation-based rate-adaptivity leads to significant savings in resources of up to 13% (8%) in the number of required LPs for Germany (EU), making it a cost-efficient solution for capacity scaling in optical networks. The savings in required LPs increase in multi-band scenarios as shown on the EU topology from 8% for C-band up to 15% for C+L+S-band. On the Germany topology the savings increase to up to 20% for C+L+S-band. Therefore, PS-QAM configurations are an effective tool to delay band upgrades of the OLS and improve the cost and power consumption scaling. The results for different symbol rate granularities show that a 12.5 GHz granularity reduces underprovisioning in C-band networks by up to 4% while a further increased granularity of 3.125 GHz offers negligible additional benefits. The results highlight the benefits of PS-QAM in terms of capacity. In addition to the capacity gains, the potential impact of increased complexity on transceiver cost and power consumption needs to be further investigated.

REFERENCES

1.   Acacia, "Acacia Unveils Industry's First Single Carrier 1.2T Multi-

Haul Pluggable Module," https://acacia-inc.com/blog/acacia-unveils-industrys-first-single-carrier-1-2t-multi-haul-pluggable-module/ (2022).

2. Acacia, "Network Optimization in the 600G Era," https://acacia-inc.com/wp-content/uploads/2018/12/Network-Optimization-in-the-600G-Era-WP1218.pdf (2018).

3. J. Cho and P. J. Winzer, "Probabilistic constellation shaping for optical fiber communications," J. Light. Technol. **37**, 1590–1607 (2019).

4. D. A. A. Mello, A. N. Barreto, T. C. de Lima, T. F. Portela, L. Beygi, and J. M. Kahn, "Optical Networking With Variable-Code-Rate Transceivers," J. Light. Technol. **32**, 257–266 (2014).

5. A. Ferrari, M. Cantono, U. Waheed, A. Ahmad, and V. Curri, "Networking Benefits of Advanced DSP Techniques and Hybrid Fiber Amplification," in *2017 19th International Conference on Transparent Optical Networks (ICTON),* (2017), pp. 1–4.

6. O. Karandin, F. Musumeci, O. Ayoub, A. Ferrari, Y. Pointurier, and M. Tornatore, "Quantifying Resource Savings from Low-Margin Design in Optical Networks with Probabilistic Constellation Shaping," in *2021 European Conference on Optical Communication (ECOC),* (2021), pp. 1–4.

7. J. Slovak, W. Schairer, M. Herrmann, K. Pulverer, and E. Torrengo, "Benefits of Performance Awareness in Coherent Dynamic Optical Networks," in *2018 Optical Fiber Communications Conference and Exposition (OFC),* (2018), pp. 1–3.

8. J. Perello, J. M. Gene, and S. Spadaro, "Evaluation of Probabilistic Constellation Shaping Performance in Flex Grid over Multicore Fiber Dynamic Optical Backbone Networks [Invited]," J. Opt. Commun. Netw. **14**, B1–B10 (2022).

9. S. Yan, F. N. Khan, A. Mavromatis, D. Gkounis, Q. Fan, F. Ntavou, K. Nikolovgenis, F. Meng, E. H. Salas, C. Guo, C. Lu, A. P. T. Lau, R. Nejabati, and D. Simeonidou, "Field trial of Machine-Learning-assisted and SDN-based Optical Network Planning with Network-Scale Monitoring Database," in *2017 European Conference on Optical Communication (ECOC),* (2017), pp. 1–3.

10. F. Shirin Abkenar and A. Ghaffarpour Rahbar, "Study and Analysis of Routing and Spectrum Allocation (RSA) and Routing, Modulation and Spectrum Allocation (RMSA) Algorithms in Elastic Optical Networks (EONs)," Opt. Switch. Netw. **23**, 5–39 (2017).

11. H. Beyranvand and J. A. Salehi, "A quality-of-transmission aware dynamic routing and spectrum assignment scheme for future elastic optical networks," J. Light. Technol. **31**, 3043–3054 (2013).

12. S. K. Patri, A. Autenrieth, J.-P. Elbers, and C. Mas-Machuca, "Multi-Band Transparent Optical Network Planning Strategies for 6G-ready European Networks," Opt. Fiber Technol. **74**, 103118 (2022).

13. B. C. Chatterjee, N. Sarma, and E. Oki, "Routing and spectrum allocation in elastic optical networks: A tutorial," IEEE Commun. Surv. & Tutorials **17**, 1776–1800 (2015).

14. J. Pedro, N. Costa, and S. Pato, "Optical Transport Network Design Beyond 100 Gbaud [Invited]," J. Opt. Commun. Netw. **12**, A123–A134 (2020).

15. J. Müller, G. Di Rosa, T. Fehenberger, M. Wenning, S. K. Patri, J.-P. Elbers, and C. Mas-Machuca, "On the Benefits of Rate-Adaptive Transceivers: A Network Planning Study," in *27th International Conference on Optical Network Design and Modelling (ONDM),* (2023).

16. R. K. Jana, M. A. Iqbal, N. Parkin, A. Srivastava, A. Mishra, J. Balakrishnan, P. Coppin, A. Lord, and A. Mitra, "Multi-fiber vs. ultra-wideband upgrade: A techno-economic comparison for elastic optical backbone network," in *European Conference on Optical Communication (ECOC) 2022,* (Optica Publishing Group, 2022), p. We1A.5.

17. R. Emmerich, M. Sena, R. Elschner, C. Schmidt-Langhorst, I. Sackey, C. Schubert, and R. Freund, "Enabling S-C-L-Band Systems With Standard C-Band Modulator and Coherent Receiver Using Coherent System Identification and Nonlinear Predistortion," J. Light. Technol. **40**, 1360–1368 (2022).

18. M. Mehrabi, H. Beyranvand, and M. J. Emadi, "Multi-band elastic optical networks: Inter-channel stimulated raman scattering-aware routing, modulation level and spectrum assignment," J. Light. Technol. **39**, 3360–3370 (2021).

19. N. Sambo, A. Ferrari, A. Napoli, N. Costa, J. Pedro, B. Sommerkorn-Krombholz, P. Castoldi, and V. Curri, "Provisioning in multi-band optical networks," J. Light. Technol. **38**, 2598–2605 (2020).

20. A. Souza, R. Sadeghi, B. Correia, N. Costa, A. Napoli, V. Curri, J. Pedro, and J. Pires, "Optimal pay-as-you-grow deployment on s+c+l multi-band systems," in *2022 Optical Fiber Communications Conference and Exhibition (OFC),* (2022), pp. 1–3.

21. B. Correia, R. Sadeghi, E. Virgillito, A. Napoli, N. Costa, J. Pedro, and V. Curri, "Networking performance of power optimized c+l+s multiband transmission," in *GLOBECOM 2020 - 2020 IEEE Global Communications Conference,* (2020), pp. 1–6.

22. H. Buglia, M. Jarmolovičius, A. Vasylchenkova, E. Sillekens, L. Galdino, R. I. Killey, and P. Bayvel, "A closed-form expression for the gaussian noise model in the presence of inter-channel stimulated raman scattering extended for arbitrary loss and fibre length," J. Light. Technol. pp. 1–10 (2023).

23. B. Correia, R. Sadeghi, E. Virgillito, A. Napoli, N. Costa, J. Pedro, and V. Curri, "Power control strategies and network performance assessment for c+l+s multiband optical transport," J. Opt. Commun. Netw. **13**, 147–157 (2021).

24. D. Semrau, R. I. Killey, and P. Bayvel, "A closed-form approximation of the gaussian noise model in the presence of inter-channel stimulated raman scattering," J. Light. Technol. **37**, 1924–1936 (2019).

25. C. Mas-Machuca, J. Müller, M. Wenning, and S. K. Patri, "Planning and Optimization of Optical Networks Based on Emerging Technologies," in *2023 European Conference on Optical Communications (ECOC),* (2023).

26. Recommendation ITU-T G.652, "Series G: transmission systems and media, digital systems and networks," (2016).

27. ADVA, "*TeraFlex™*," https://www.adva.com/en/products/open-optical-transport/fsp-3000-open-terminals/teraflex. [Last accessed: January 2023].

28. Zuse Institute Berlin, "SNDlib Problem Instances," http://sndlib.zib.de/, Accessed: 2023-01-17.

29. D. S. Millar, T. Fehenberger, T. Koike-Akino, K. Kojima, and K. Parsons, "Distribution matching for high spectral efficiency optical communication with multiset partitions," J. Light. Technol. **37**, 517–523 (2019).

30. J. Cho and P. J. Winzer, "Probabilistic constellation shaping for optical fiber communications," J. Light. Technol. **37**, 1590–1607 (2019).

31. J. Cho, S. L. I. Olsson, S. Chandrasekhar, and P. Winzer, "Information Rate of Probabilistically Shaped QAM with Non-Ideal Forward Error Correction," in *2018 European Conference on Optical Communication (ECOC),* (2018), pp. 1–3.

32. A. Alvarado, E. Agrell, D. Lavery, R. Maher, and P. Bayvel, "Replacing the Soft-Decision FEC Limit Paradigm in the Design of Optical Communication Systems," J. Light. Technol. **34**, 707–721 (2016).

33. T. Yoshida, M. Karlsson, and E. Agrell, "Performance Metrics for Systems With Soft-Decision FEC and Probabilistic Shaping," IEEE Photonics Technol. Lett. **29**, 2111–2114 (2017).

34. D. Semrau, E. Sillekens, R. I. Killey, and P. Bayvel, "A modulation format correction formula for the gaussian noise model in the presence of inter-channel stimulated raman scattering," J. Light. Technol. **37**, 5122–5131 (2019).